

Effect of CdS and In₃Se₄ BSF layers on the photovoltaic performance of PEDOT:PSS/n-Si solar cells: Simulation based on experimental data

Bipanko Kumar Mondal ^a, Shaikh Khaled Mostaque ^a, Md. Abdur Rashid ^{a,b}, Abdul Kuddus ^{a,c}, Hajime Shirai ^c, Jaker Hossain ^{a,*}

^a Solar Energy Laboratory, Department of Electrical and Electronic Engineering, University of Rajshahi, Rajshahi, 6205, Bangladesh

^b Department of Physics, University of Rajshahi, Rajshahi, 6205, Bangladesh

^c Graduate School of Science and Engineering, Saitama University, Saitama, 338-8570, Japan



ARTICLE INFO

Keywords:

PEDOT:PSS/n-Si solar Cells
CdS and In₃Se₄ BSF
Bulk defects
Photovoltaics
SCAPS-1D simulation

ABSTRACT

In this article, we perform a theoretical analysis on PEDOT:PSS/n-Si heterojunction solar cells for further enhancement of the solar cells. We introduced CdS and In₃Se₄ chalcogenide compounds as back surface field (BSF) layer in the solar cell. The impacts of various parameters such as the thickness, doping and defect densities on the photovoltaic performance have been investigated in details employing the solar cell capacitance simulator (SCAPS-1D) software. It is found that the power conversion efficiency (PCE) of the PEDOT:PSS/n-Si heterojunction solar cells significantly increases with use of these BSF layers. The optimized PCE of the PEDOT:PSS/n-Si solar cell is 22.46% which increases to 30.94% with V_{OC} = 0.89 V, J_{SC} = 44.02 mA/cm² and FF = 78.92%, respectively due to the use of CdS BSF layer. On the other hand, the PCE of the solar cell is found to be 38% with V_{OC} = 0.84 V, J_{SC} = 53.22 mA/cm² and FF = 85.11%, respectively as a result of longer wavelength absorption in In₃Se₄ BSF layer. These entire theoretical predictions indicate the promising applications of CdS and In₃Se₄ compounds as BSF layers in PEDOT:PSS/n-Si heterojunction solar cells to harness solar energy in near future.

1. Introduction

Solution-processed PEDOT:PSS/n-Si heterojunction solar cells have appeared as one of the most potentials candidate of low cost renewable energy sources to meet the increasing global energy demand by combining the low cost solution-processed organic materials and the high efficiency of silicon solar cell [1–5]. The efficiency of this type of solar cells has succeeded to 13–20% [6–10]. Recently, the modules of all solution-processed PEDOT:PSS/n-Si solar cell with two different sizes of 2 × 2 cm² and 4 inch have been demonstrated exhibiting an output power of 0.37 W and 7.3 W with an efficiency of 13–14% and 11–12%, respectively [11].

So far, different techniques have been employed to further improve the efficiency of PEDOT:PSS/n-Si solar cells such as modifying the conductivity of PEDOT:PSS [12], reducing the resistivity of Si [13], lowering the work-function of Si/cathode contact by incorporating thin film materials such as Mg [14], SiO₂/Mg stack [15], LiF [16], Cs₂CO₃ [5,17], Ba(OH)₂ [18], perylene diimide (PDIN) [19], TiO_x [20], organic materials 8-hydroxyquinolinolato-lithium (Liq) [21], NDI-based polymer poly{[N,NO-bis

* Corresponding author.

E-mail address: jak_appee@ru.ac.bd (J. Hossain).

(2-octyldodecyl)-naphthalene-1,4,5,8-bis(dicarboximide)-2,6-diyl]-alt-5,50-(2,20-bithiophene)} [P(NDI2OD-T2)]; Polyera ActivInk N2200] (N2200) [22] and amino acids [23] etc. These thin film materials lower the work function by interface dipolar effect or acting as back surface field (BSF) which attributes to the efficiency enhancement by decreasing minority carrier recombination and increasing majority carrier transport. The anti-reflection coatings (ACRCs) with solution-processed TiO₂, MoO_x and Nafion on the top of PEDOT: PSS has also been applied for PEDOT:PSS/c-Si heterojunction solar cells for the enhancement of the devices [2,6–8]. The reflectance of the solar cells was also reduced by texturing the silicon which enhances the short circuit current, but this techniques are not suitable for the PEDOT:PSS/n-Si solar cells as it significantly introduces defects at the PEDOT:PSS/n-Si interface resulting lower open circuit voltage and hence photovoltaic performance of the solar cell [2,24,25]. However, unfortunately, none of these techniques could provide a compatible efficiency with existing silicon solar cells which already shows a highest efficiency of 26.33% with a practical module size of 180 cm² [26]. Therefore, a different approach is necessary for further enhancement of the efficiency of the PEDOT: PSS/n-Si heterojunction solar cells.

In addition, the Shockley–Queisser (SQ) efficiency limit of a dual-heterojunction (DH) solar cell is 42–46% [27,28]. Moreover, the intermediate band solar cell which operates with two-step photon upconversion process has the SQ limit of about 63% [29]. Besides, the impurity photovoltaic (IPV) which enhances the photocurrent by the absorption of low energy sub-band photon by two-step photon upconversion shows a theoretical efficiency of 77.2% [30]. In fact, a simulation result on Si IPV solar cell shows an efficiency of 29.3% with a J_{sc} of about 49 mA/cm² [31]. However, there is no report of such high efficiency DH solar cells even in simulation that reach SQ limit.

Herein, we introduce the highly conductive CdS and In₃Se₄ thin film as BSF layer for the enhancement of efficiency of the PEDOT: PSS/n-Si heterojunction solar cells. CdS is an n-type semiconductor with a band gap of 2.4 eV which has been reported to be fabricated by low-cost solution process indicating its potential in future solution-processed solar cells applications [32]. Recently, it has been employed for the deposition of n-CdS/p-Si heterojunction solar cells which already shows an efficiency of 12.29% [33]. On the other hand, In₃Se₄ is a new n-type highly degenerate semiconducting 2D compound consisting of alternating Se-In-Se-In–Se-In-Se and stack along the [0001] direction [34–36]. Recently, we have reported the potentials of metallic In₃Se₄ with an optical band gap of 1.8 eV as emitter in the chalcogenide/p-Si solar cells [37]. More recently, In_{2.45}Se₄ phase with a band gap of ~1.53 eV has also been reported [38]. Moreover, it is also reported that indium selenide thin films like other chalcogenides can also be deposited by solution process which opens the potential of low-cost solar cell fabrication [39].

In this article, we theoretically demonstrate the utilization of CdS and In₃Se₄ as back surface field (BSF) layers in PEDOT:PSS/n-Si solar cells in details employing the experimental data. The effect of different physical parameters of PEDOT:PSS, Si and BSF layers on the photovoltaic performances have been investigated for the designed solar cells. This study reveals that the incorporation of CdS and In₃Se₄ BSF layers are highly promising for the highly efficient PEDOT:PSS/n-Si heterojunction solar cells.

2. Experimental details

2.1. Thin film preparation and characterization

Thin films of PEDOT:PSS, CdS and In₃Se₄ were deposited on the glass substrates for the measurement of transmittance and carrier concentration. The glass substrates were firstly washed with piranha solution to avoid gross contamination and then cleaned with acetone, isopropyl alcohol (IPA) and deionized (DI) water each for 10 min, respectively and dried with an air blower before the film deposition.

Conductive PEDOT:PSS (Clevios PH1000) with 7 wt% Ethylene glycol (EG) and 0.2 wt% Zonyl surfactant was spin coated on the glass substrate at 2500 rpm for 1 min. Then the samples were annealed at a temperature of 140 °C for 30 min to drive away the residual solvent.

The CdS thin films were deposited on glass substrate by spin coating method from a precursor which was prepared by dissolving CdS powder in Triton X-100 added thiol-amine cosolvents. The films were pre-annealed at 90 °C for 10 min followed by high temperature annealing at 250–350 °C for 3–7 min, respectively for the crystallization of the films. The experimental details can be found in other work [32].

Indium selenide thin films were deposited by e-beam evaporation technique onto glass substrate at room temperature at a pressure of ~8 × 10⁻⁵ Pa. The as-deposited films were annealed at ~200 °C to a get In₃Se₄ phase as it was confirmed that as-deposited films encounter a transition from In₂Se₃ to In₃Se₄ phase due to annealing. The experimental details can be found in other work [36].

The thicknesses of the PEDOT:PSS and CdS films were measured by the DekTak XTL thickness profiler whereas that of In₃Se₄ was measured by an optical method and was verified by cross-sectional SEM study. The carrier concentration of the films was measured by four-probe method. The transmittance of the films were recorded by Shimadzu UV-VIS spectrophotometer (UV-2600 Shimadzu) and T-60 ultraviolet-visible (UV-vis) Spectrophotometer (PG Instruments).

2.2. Device simulation

SCAPS (Solar Cell Capacitance Simulator) simulation software was used for the simulation of PEDOT:PSS/n-Si heterojunction solar cells [40–43]. The designed structure was simulated under one sun illumination (100 mW cm⁻²) and global air mass (AM) 1.5 spectrum at a temperature of 300 K considering ideal values for series (Rs) and Shunt (Rsh) resistance. The recombinations and charge states were considered only in the bulk materials and defects were considered at the layers interfaces. Using the Gaussian energetic distribution the single acceptor and donor defects were distributed in the bulk layer. In this simulation, Ni and Al were used as front

and rear metal contacts. The transmittance spectra (T) of PEDOT:PSS, CdS and In_3Se_4 thin films used in this study are shown in Fig. 1. The absorption coefficient (α) used in the simulation has been calculated from the following equation [32].

$$\alpha = \frac{\ln(\frac{1}{T})}{t} \quad (1)$$

where, t is the thickness of the corresponding thin films.

The band gap, carrier concentration and other parameters used in this simulation were acquired from the experimental data and reported works [32,36,37,43,44]. Table 1 shows the simulation parameters employed in this study for the characterization of PEDOT:PSS/n-Si device whereas, Table 2 shows the defect parameters for the PEDOT:PSS/Si, Si/CdS and Si/ In_3Se_4 interfaces.

3. Results and discussion

3.1. PEDOT:PSS/n-Si solar cells with and without BSF layer

The schematic structure and illuminated energy band diagram of PEDOT:PSS/n-Si heterojunction solar cell, respectively are shown in Fig. 2a and b. The PEDOT:PSS polymer is a p-type degenerate semiconductor with a band gap of 1.6 eV. The HOMO and LUMO of this polymer are 3.55 and 5.15 eV, respectively. On the other hand, the band gap of Si is 1.12 eV and E_C and E_V of this semiconductor are 4.05 and 5.17 eV, respectively. Therefore, PEDOT:PSS forms a suitable pn junction with Si. The device operation of PEDOT:PSS/n-Si heterojunction solar cell is based on charge selective n-type Si and the synthetic hole-conducting p-type metal PEDOT:PSS as schematically shown in the figure. The photo-generated holes at the silicon pass through the junction and are collected by the anode and photo-generated electrons are blocked by the PEDOT:PSS layer due to higher LUMO and collected by the cathode.

However, CdS has a band gap of 2.4 eV and its electron affinity varies from 4.2 to 4.5 eV [32,33,43]. Therefore, highly conductive CdS can form a suitable junction with silicon. Similarly, the Fermi energy (E_F) and electron affinity of In_3Se_4 are about ~ 4.4 eV and 4.55 eV, respectively [36,45]. As a result, In_3Se_4 can also build a favourable junction with silicon. Therefore, both the CdS and In_3Se_4 can act as BSF layers for PEDOT:PSS/n-Si heterojunction solar cells.

3.1.1. Built-in potential of PEDOT:PSS/n-Si/CdS(In_3Se_4) heterojunction

The p-PEDOT:PSS/n-Si/ n^+ - In_3Se_4 or p-PEDOT:PSS/n-Si/ n^- -CdS solar cells are formed with two heterojunctions (p/n and n/ n^+) with the doping density N_A in p-absorber, N_D in n-window and N_d in n^+ -BSF layers, respectively. The built-in potential (ψ_{p-n}) of the hetero p-n junction can be calculated using the following Eq (2) [46],

$$\psi_{p-n} = \frac{\Delta E_C - \Delta E_V}{2q} + \frac{KT}{q} \ln \frac{N_D N_A}{n_{i,n} n_{i,p}} + \frac{KT}{2q} \ln \frac{N_{v,n} N_{c,p}}{N_{c,n} N_{v,p}} \quad (2)$$

where, N_C and N_V denote the effective DOS at CB and VB edges, KT presents the thermal voltage, q is the electron charge and $n_{i,n}$ and $n_{i,p}$ represent the intrinsic carrier concentration of the p-type PEDOT:PSS ($3 \times 10^{20} \text{ cm}^{-3}$) [44] and n-type Si ($1.08 \times 10^{10} \text{ cm}^{-3}$) [47] layers, respectively. The built-in potential (ψ_{n^+-n}) of the n^+ -n junction can be calculated from the following Eq (3) [46],

$$\psi_{n^+-n} = \frac{\Delta E_C - \Delta E_V}{2q} + \frac{KT}{q} \ln \frac{N_d N_D}{n_{i,p} n_{i,n^+}} + \frac{KT}{2q} \ln \frac{N_{v,n} N_{c,n^+}}{N_{c,n} N_{v,n^+}} \quad (3)$$

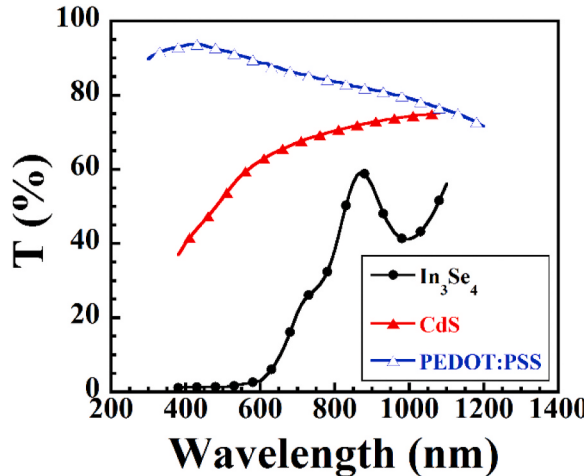


Fig. 1. Transmittance spectra of PEDOT:PSS (100 nm), CdS (300 nm) and In_3Se_4 (250 nm) thin films deposited on glass substrates by spin coating and Electron beam evaporation techniques, respectively.

Table 1Simulation parameters used for the PEDOT:PSS/n-Si/n⁺-CdS or n⁺-In₃Se₄ heterojunction solar cells at 300 K.

Parameters	n-Si [37]	PEDOT:PSS [44]	CdS [43]	In ₃ Se ₄ [37]
Layer type	Absorber	Window	BSF	BSF
Conductivity type	<i>N</i>	<i>P</i>	<i>N⁺</i>	<i>N⁺</i>
^a Thickness [μm]	150	0.10	0.20	2.0
Band gap, <i>E_G</i> [eV]	1.12	1.6	2.4	1.8
Electron affinity, χ [eV]	4.05	3.55	4.4	4.55
Dielectric permittivity, ϵ [relative]	11.9	2.58	10	5.54
Effective CB density, <i>N_C</i> [cm ⁻³]	2.8×10^{19}	2.1×10^{21}	2.2×10^{18}	1.0×10^{18}
Effective VB density, <i>N_V</i> [cm ⁻³]	1.04×10^{19}	2.0×10^{21}	1.8×10^{19}	1.0×10^{18}
Electron mobility, μ_e [cm ² V ⁻¹ s ⁻¹]	1350	1	100	100
Hole mobility, μ_h [cm ² V ⁻¹ s ⁻¹]	500	20	25	50
^a Donor concentration, <i>N_D</i> [cm ⁻³]	10^{16}	0	10^{18}	10^{21}
^a Acceptor concentration, <i>N_A</i> [cm ⁻³]	0	3.0×10^{20}	0	0
Defect type	Acceptor	Acceptor	Acceptor	Acceptor
Energetic distribution	Gaussian	Gaussian	Gaussian	Gaussian
Peak defect density, <i>N(t)</i> [eV ⁻¹ cm ⁻³]	10^{11}	10^{14}	10^{14}	10^{14}
Characteristic energy [eV]	0.01	0.1	0.1	0.1
Reference energy [eV]	0.56	0.8	1.2	0.9
Electron capture cross section for acceptor defect [cm ²]	10^{-17}	10^{-17}	10^{-17}	10^{-17}
Hole capture cross section for acceptor defect [cm ²]	10^{-15}	10^{-15}	10^{-15}	10^{-15}

^a Is a variable field. The numbers in the [] indicates the reference numbers.**Table 2**

Interface parameters used in this simulation.

Parameters	PEDOT:PSS/Si interface	Si/CdS interface	Si/In ₃ Se ₄ interface
Defect type	Neutral	Neutral	Neutral
Capture cross section for electrons [cm ²]	10^{-19}	10^{-19}	10^{-19}
Capture cross section for holes [cm ²]	10^{-19}	10^{-19}	10^{-19}
Energetic distribution	Single	Single	Single
Reference for defect energy level E _t	Above the highest E _V	Above the highest E _V	Above the highest E _V
Energy with respect to reference (eV)	0.6	0.6	0.6
Total defects (cm ⁻²)	10^{10}	10^{10}	10^{10}

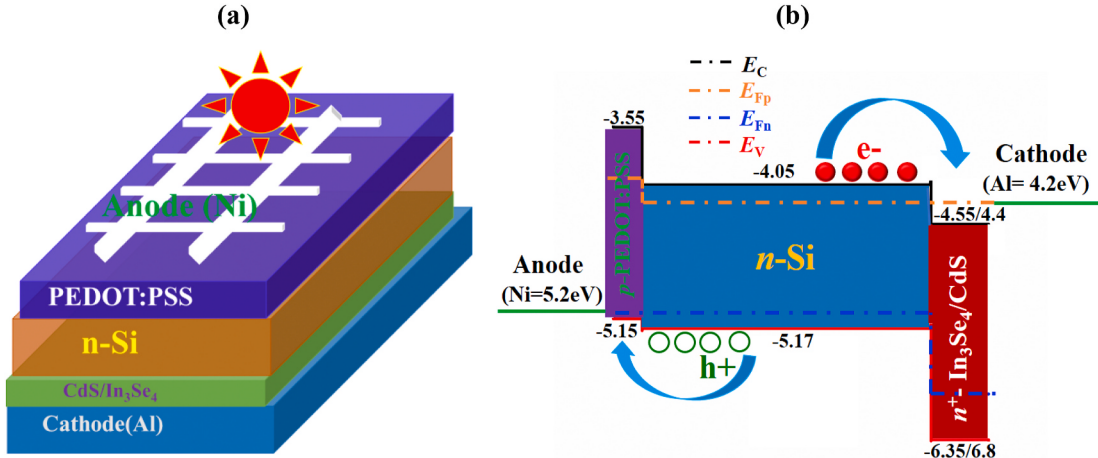


Fig. 2. The (a) schematic structure and (b) illuminated energy band diagram of PEDOT:PSS/n-Si heterojunction solar cells.

where, $n_{i,n}^+$ deontes the intrinsic carrier concentration of the CdS ($1.19 \times 10^{19} \text{ cm}^{-3}$) [44] or In₃Se₄ (1×10^{21}) layer [36,37]. Therefore, the built-in potential (ψ) for the *p*-PEDOT:PSS/n-Si/n⁺-In₃Se₄ or *p*-PEDOT:PSS/n-Si/n⁺-CdS heterojunction solar cell can be found as Eq (3),

$$\psi = \psi_{p-n} + \psi_{n-n^+} \quad (4)$$

The calculated built-in potentials for the *p*-PEDOT:PSS/n-Si/n⁺-In₃Se₄ or *p*-PEDOT:PSS/n-Si/n⁺-CdS heterojunctions are shown in

Table 3. It is seen from the table the both CdS and In₃Se₄ generates strong field with silicon.

3.2. Impact of absorber and window layer on PV parameters

3.2.1. Effect of Si absorber layer

In this section, the effects of thickness, carrier concentration and defect density of Si absorber layer on PEDOT:PSS/n-Si solar cell have been discussed. Fig. 3a delineates the PV performance of PEDOT:PSS/Si solar cell with respect to thickness of Si considering 10¹⁶ and 10¹¹ as carrier and defects density, respectively. The short circuit current (J_{SC}) is found to increase from 40.61 mA/cm² at thickness 100 μm to 43.23 mA/cm² at thickness 300 μm. The short circuit current increases because thicker absorber layer can absorb more photons and creates more electron-hole pairs (EHPs) [46,48].

The open circuit voltage (V_{OC}) also increases by a negligible amount with increasing thickness of absorber layer. It increases from 0.64 V at thickness 100 μm to 0.66 V at thickness 300 μm. The fill factor (FF) has insignificant changes from 83.37 to 83.80% due to increasing thickness of Si from 100 to 300 μm. The power conversion efficiency (PCE) is also raised as usual from 21.50 to 24.04% with increasing absorber layer thickness from 100 to 300 μm due to increment of others parameters.

The quantum efficiency (QE) as function of the photon wavelength (λ) is the ratio of number of charge carriers collected by the solar cell to the incident photons on that cell [46,49]. Fig. 3b depicts the effect of the variation of thickness of Si on quantum efficiency. The QE has slight increment due to the thicker absorber layer because of absorbing more photons. At lower wavelength it is almost independent but at higher it decreases towards 0% because of photon energy, $h\nu < \text{band gap } E_g$.

Fig. 4a and b shows the influences of carrier and defect density of Si absorber layer on PEDOT:PSS/Si solar cell considering thickness of 150 μm. It is noticed from Fig. 4a that V_{OC} increases from 0.59 to 0.70 V with increasing doping concentration from 10¹⁴ to 10¹⁷ cm⁻³. But at the same time, J_{SC} decreases. It decreases from 43.81 to 41.49 mA/cm² owing to increase in donor concentration from 10¹⁴ to 10¹⁷ cm⁻³ on account of the recombination losses which might occur as a result of high carrier concentration [50,51]. The FF ameliorates also with carrier concentration of Si layer from 80.57 to 84.61% due to the decrease of series resistance. Furthermore, PCE increases from 20.90 to 24.68% at the increase in donor concentration from 10¹⁴ to 10¹⁷ cm⁻³, respectively. We have considered 150 μm and 10¹⁶ cm⁻³, respectively as the optimized thickness and donor concentration for Si to carry out further investigations.

To investigate cell dependency on bulk defects of Si absorber layer, defect level was varied from 10⁹ to 10¹³ cm⁻³ and found that all the PV parameters are almost unchanged up to 10¹² cm⁻³. However, further increase in defects significantly affects the PV parameters of the solar cell as shown in Fig. 4b. This is happened because of higher defects level which obstructs the collection of photo-generated carriers therefore reduced photocurrent.

3.2.2. Effect of PEDOT:PSS window layer

In this section, we report the influences of PEDOT:PSS window layer on PEDOT:PSS/n-Si heterojunction solar cells. Fig. 5a and b shows the PV performances of PEDOT:PSS/Si solar cells with respect to thickness and defect density, respectively of PEDOT:PSS window layer. The thickness of PEDOT:PSS was varied from 0.1 to 0.5 μm. From Fig. 5a, it is observed that V_{OC} and FF are almost independent with the thickness of window layer. But J_{SC} firstly increases up to 0.3 μm but then it abated again. The PCE also follows this trend. The decrement of J_{SC} with thicker window layer is reasonable because it obstructs lower wavelength photons to reach the absorber layer by parasitic absorption which in turn reduces the output current. However, a recent investigation shows that an anti-reflection coating (ARC) layer on the top of PEDOT:PSS polymer can effectively reduce the front reflection of light in the PEDOT:PSS/n-Si solar cells which will increase current as well as efficiency of the solar cells [52].

Fig. 5b depicts that V_{OC} is almost independent with defect density of PEDOT:PSS window layer and is nearly 0.65 V. The J_{SC} is also almost independent with defect density up to 10¹⁵ cm⁻³. After that, it decreases to 40.85 from 41.66 mA/cm² with increasing defect level from 10¹² to 10¹⁶ cm⁻³. The FF is also immutable with defect density of PEDOT:PSS. Herein, PCE is depended on J_{SC} only and has trivialize decrement from 22.47 to 22% after 10¹⁵ cm⁻³ of defects of PEDOT:PSS window layer. Therefore, we can conclude that defect density of PEDOT:PSS window layer has ignorable effect on output parameters of PEDOT:PSS/Si solar cells.

3.3. Effect of CdS BSF layer on PV performance

To investigate the effect of CdS as BSF layer on PEDOT:PSS/n-Si solar cell, thickness, doping concentration and defect density were varied. Fig. 6 exhibits the contour plots of PV performance with the variation of thickness and doping concentration of CdS BSF layer considering 10¹⁴ as defect density. Additionally, employing 200 nm CdS BSF layer the efficiency of the solar cell is improved to 30.94% with V_{OC} of 0.89 V, J_{SC} of 44.02 mA/cm² and FF of 78.92% keeping all the parameters unchanged.

Table 3

Built-in potentials for PEDOT:PSS/n-Si/(n⁺-CdS or n⁺-In₃Se₄) heterojunction solar cells.

Junctions	Built-in potential 1 $V_{bi(PEDOT/Si)}$ (V)	Built-in potential 2 $V_{bi(n-Si/CdS \text{ or } In_3Se_4)}$ (V)	Device Built-in potential, V_{bi} (V)
p-PEDOT:PSS/n-Si	0.84	–	0.84
p-PEDOT:PSS/n-Si/n ⁺ -CdS	0.84	1.16	2.0
p-PEDOT/n-Si/n ⁺ -In ₃ Se ₄	0.84	1.08	1.92

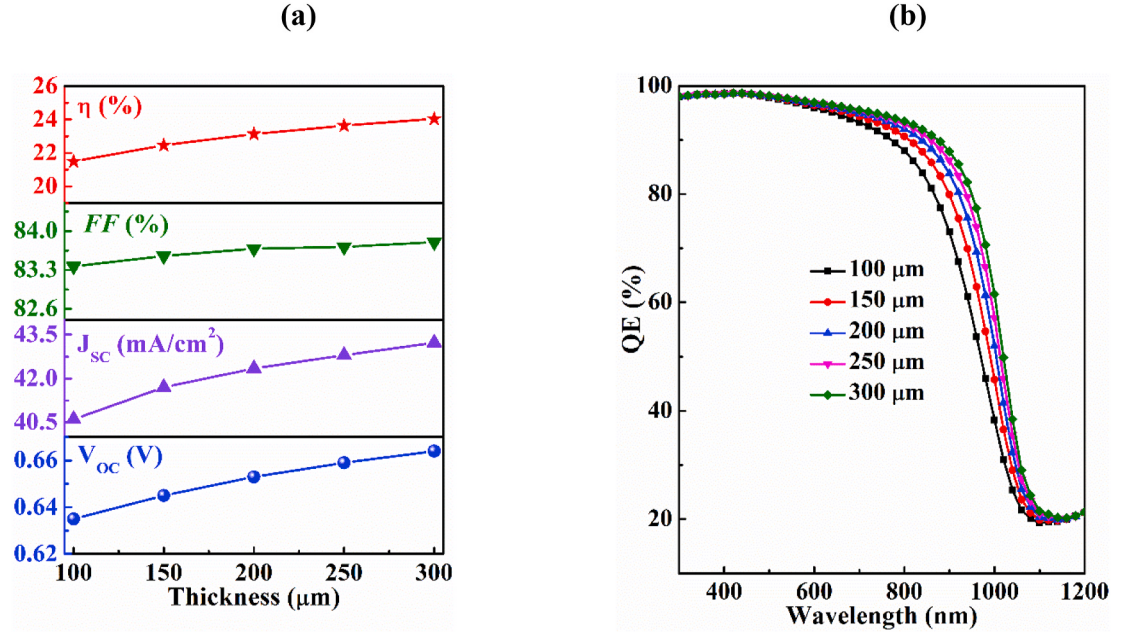


Fig. 3. (a) Variation of PV parameters of PEDOT:PSS/Si solar cells with respect to absorber layer thickness and (b) The effect of absorber layer thickness on quantum efficiency.

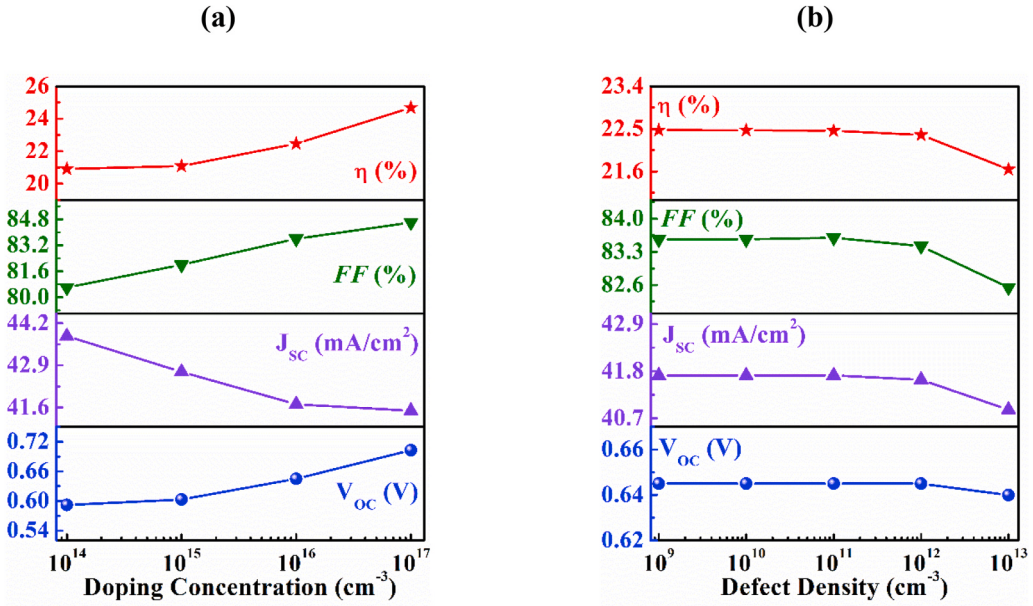


Fig. 4. Variation of PV parameters of PEDOT:PSS/Si solar cells with respect to (a) carrier concentration and (c) defect density of absorber layer.

The J_{SC} increases from the pristine case due to the decrease in surface recombination velocity at the interface by strong field of the BSF layer that reduces recombination current. But interestingly, it could not be improved further with increasing thickness of CdS layer due to its high band gap and it reached to 44.03 mA/cm^2 at $> 10^{19} \text{ cm}^{-3}$ which is shown in Fig. 6a.

The V_{OC} of PEDOT:PSS/n-Si heterojunction solar cells is 0.65 V without CdS BSF layer. The V_{OC} of the devices increases by 0.24 V due to the insertion of CdS BSF layer. The origin of this increment V_{OC} mainly due to insertion of highly degenerate CdS BSF layer which in turn generates the high built-in potential of 2.0 V resulting the increment of the open circuit voltage as discussed in section 3.1.1 [46, 49]. It is also viewed in Fig. 6b that V_{OC} is also increased with donor concentration $> 10^{19} \text{ cm}^{-3}$ and it is independent on thickness of CdS layer. As both J_{SC} and V_{oc} are independent with thickness of CdS, FF and PCE are also found to constant with thickness but

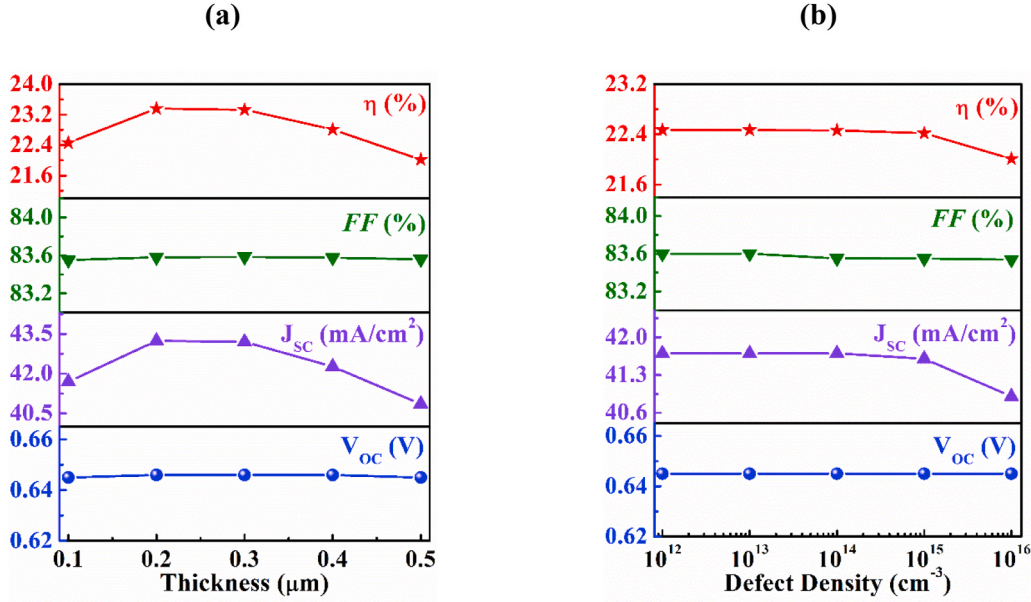


Fig. 5. Variation of PV parameters of PEDOT:PSS/Si solar cells with respect to (a) thickness and (b) defects of window layer.

enhanced to 83.97 and 33.65%, respectively only for highly doping $> 10^{19} \text{ cm}^{-3}$.

Hence, it is summarized that the cell performance remain unchanged for further increasing thickness of CdS BSF layer at lower carrier concentration but it can be improved slightly through highly doping concentration $> 10^{19} \text{ cm}^{-3}$.

Fig. 7 shows contour plots for the influences of thickness and bulk defects of CdS on cell performance and observed that all PV parameters J_{SC} , V_{OC} , FF and PCE are totally independent on thickness and defect density of CdS layer.

3.4. Effect of In_3Se_4 BSF layer on PV performance

3.4.1. Impact of thickness and carrier concentration on PV parameters

In this section, the impacts of thickness and carrier concentration of In_3Se_4 BSF layer which also acts as bottom absorber layer on PEDOT:PSS/Si solar cell output parameters are explored.

Fig. 8 delineates cell dependency on thickness and carrier concentration of In_3Se_4 layer. We have varied thickness from 0.2 to 5 μm and donor concentration from 10^{17} to 10^{21} cm^{-3} . It is noticed in Fig. 8a that J_{SC} has significantly improvement with increasing thickness and doping concentration of In_3Se_4 layer. The J_{SC} is enhanced from 46.49 to 54.90 mA/cm^2 at thickness 0.2 μm with carrier concentration of 10^{17} cm^{-3} to 5 μm with 10^{21} cm^{-3} . The thicker In_3Se_4 BSF layer can absorb number of longer wavelength photons that can create more electron-hole pairs and as a result the current is highly increased [54]. The longer wavelength photon absorption by In_3Se_4 layer can be explained by Tail-States-Assisted (TSA) two-step upconversion process [55]. In TSA upconversion, the Urbach tail states in the material can participate in the absorption of two low-energy (sub-gap) photons in sequence that will create an e-h pair. A materials with high doping concentration, preferred wide band gap and high absorption coefficient in longer wavelength region may provide TSA two-step up conversion process. Having the wide band gap of 1.8 eV, doping concentration of 10^{21} cm^{-3} and absorption coefficient of 10^2 cm^{-1} (obtained from SCAPS extrapolation) in the wavelength of 1800 nm, In_3Se_4 can absorb longer wavelength photons that enhances photocurrent in PEDOT:PSS/Si solar cell.

It is observed that only 2 μm additional In_3Se_4 BSF layer on PEDOT:PSS/Si solar cell enhances the cell performance to 38% with J_{SC} of 53.22 mA/cm^2 , V_{OC} of 0.84 V and FF of 85.11% keeping carrier and defect density as 10^{21} and 10^{14} cm^{-3} , respectively.

In Fig. 8b, V_{OC} is increased from 0.77 to 0.84 V with thickness 0.2–5 μm and carrier concentration 10^{17} to 10^{21} cm^{-3} of In_3Se_4 layer. The high open circuit voltage is the consequence of the insertion of highly degenerate In_3Se_4 BSF layer which produces a higher built-in potential of 1.92 V [46,49].

The FF in Fig. 8c is found to rise from 77.11 to 85.12% with increasing thickness and carrier concentration. The PCE in Fig. 8d is also seen to rise from 27.74 to 39.2% with increasing thickness and carrier of In_3Se_4 layer. We have achieved maximum efficiency 39.2% at thickness 5.0 μm with 10^{21} carrier concentration. Therefore, we consider 10^{21} cm^{-3} as our optimized carrier concentration for our others investigations.

3.4.2. Impact of thickness and defect density

Fig. 9 shows the dependency on thickness and bulk defects of In_3Se_4 layer on PV parameters. To study the influences of defect density and thickness of In_3Se_4 layer, we have varied defect density from 10^{14} to 10^{19} cm^{-3} and thickness 0.2–5 μm . In Fig. 9a, J_{SC} is

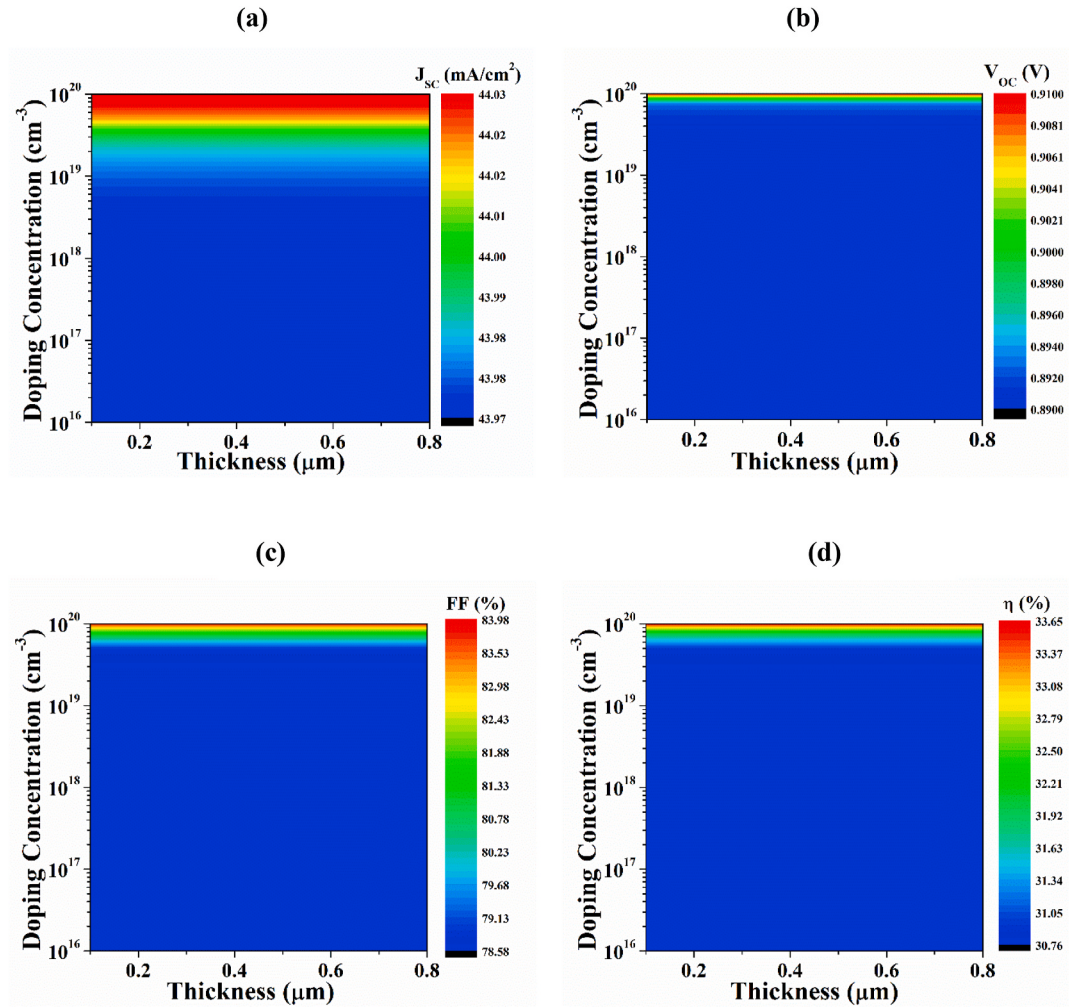


Fig. 6. Variation of PV parameters with thickness and doping concentration of CdS BSF layer: (a) J_{SC} , (b) V_{OC} (c) FF and (d) Efficiency (η).

seen to increase with thickness as usually and there is no influences of defect density $< 10^{14} \text{ cm}^{-3}$ on it. Since, the higher defect density reduces the rate of creating EHPs, at higher defects $\geq 10^{14} \text{ cm}^{-3}$ J_{SC} starts to decrease [46]. It is also visualized in Fig. 9b that there is negligible effect of defect density and thickness on V_{OC} and it is approximately 0.84 V.

Fig. 9c depicts that FF is almost independent with thickness and defect density of In_3Se_4 and it is expanded from 85.05 to 85.12% only. Finally, PCE increases with thickness whereas it decreases with defect density of In_3Se_4 layer as noticed in Fig. 9d.

3.5. The effect of BSF layer on quantum efficiency

Fig. 10a represents the simulated quantum efficiency (QE) with the variation of the thickness of CdS BSF layer. It is observed that QE firstly increases in the longer wavelength region with the insertion of the CdS layer which is resulted from the reduced surface recombination velocity in Si/CdS interface that minimizes carrier recombination due to the back surface field effect of that layer [56]. This Figure also reveals that QE is independent on thickness of CdS BSF layer. This is expected as the band gap of CdS is higher to absorb longer wavelength light as most of the shorter and visible light ($< 900 \text{ nm}$) is absorbed within $30 \mu\text{m}$ near the illuminating front silicon surface [18,53]. Therefore, increasing CdS layer thickness does not contribute to photon absorption thus photocurrent.

Fig. 10b represents the simulated quantum efficiency (QE) of PEDOT:PSS/n-Si/ In_3Se_4 solar cell with the variation of In_3Se_4 layer thickness. It is interesting to note from the figure that QE highly increases with increasing thickness of In_3Se_4 BSF as well as bottom absorber layer and in the longer wavelength region e.g. at an wavelength of 1800 nm it has quantum efficiency above 20%. This may happened as In_3Se_4 has band gap of 1.8 eV , carrier concentration of the order of 10^{21} cm^{-3} and absorption coefficient (α) of 10^2 cm^{-1} at 1800 nm that can result in absorbing longer wavelength light through TSA two-step upconversion process where two low energy photons are absorbed in sequence to make an electron-hole pair [57]. Therefore, it will also increase current as well as efficiency of the devices [54,55].

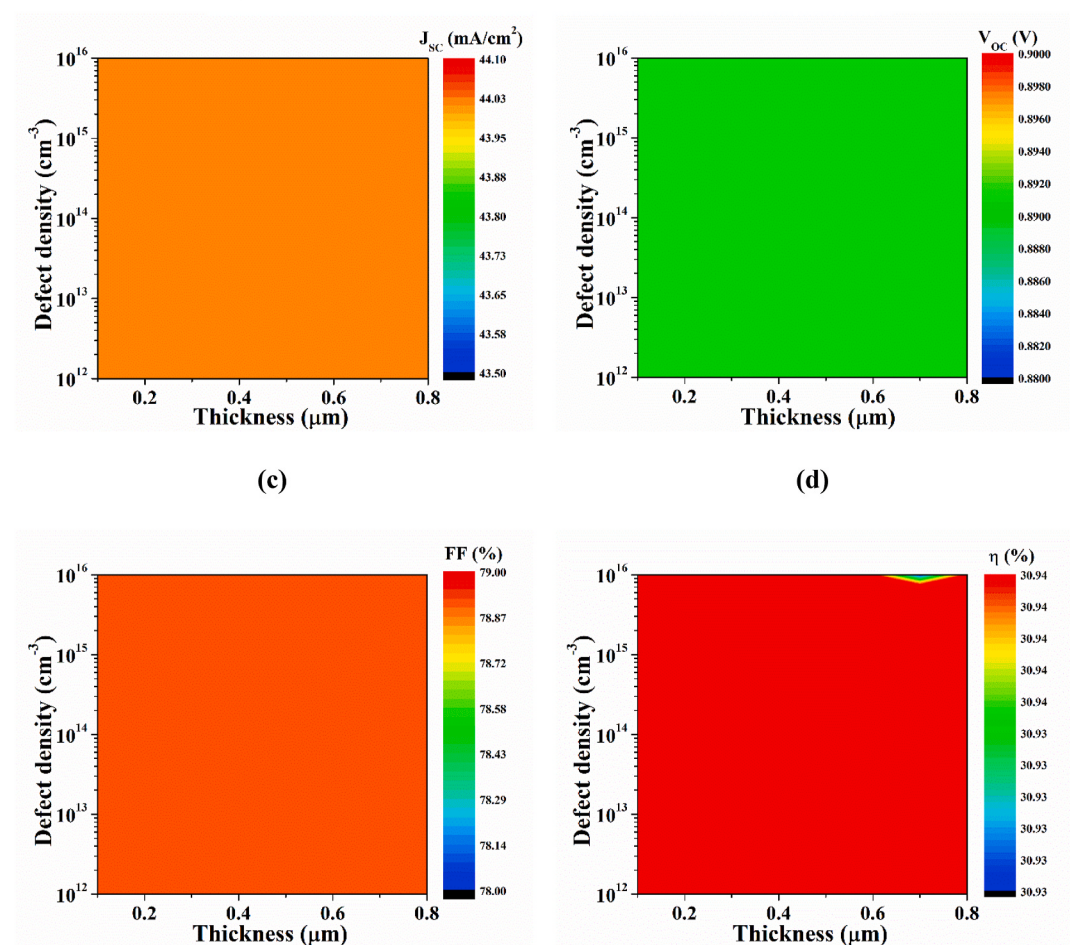


Fig. 7. Variation of PV parameters with respect to thickness and bulk defects of CdS BSF layer: (a) J_{SC} , (b) V_{OC} (c) FF and (d) Efficiency (η).

3.6. Impact of series and shunt resistance on PEDOT:PSS/Si solar cell with BSF layer

The series (R_s) and shunt (R_{sh}) resistances, which are mainly generated from the contacts among the solar cell layers, right and left side metal contacts and manufacturing defects, have considerable impacts on the solar cells performance [56]. The influences of R_s and R_{sh} on PEDOT:PSS/Si solar cell with BSF layer have been also investigated and discussed in this section.

Fig. 11 a and b represent the effect of series and shunt resistance on PEDOT:PSS/Si solar cell with CdS BSF layer, respectively. To study the effect of R_s and R_{sh} on PV performances, we have varied R_s from 1 to 5 Ω and R_{sh} from 1 to 10 K Ω , respectively. In Fig. 11a, it is seen that there is no effect of series resistance on V_{OC} and J_{SC} but FF is greatly affected. FF is reduced from 78.92 to 74.58% at $R_s = 0$ –1 Ω and it is further reduced with increasing R_s and at 5 Ω , it falls to 58.14%. As FF is greatly downturned, PCE has also large decrement to 22.80 from 30.94% due to series resistance. The V_{OC} and J_{SC} are also found constant with shunt resistance (R_{sh}) as shown in Fig. 11b. But, at the same time, firstly FF and η are slightly decreased to 77.58 and 30.37% from 78.92 to 30.94%, respectively at $R_{sh} = 0$ –1 K Ω . Then, they have further slightly increased to 78.79 and 30.88%, respectively with increasing of R_{sh} at 1 to 10 K Ω .

Fig. 11c and d delineate the effect of series and shunt resistance on PEDOT:PSS/Si solar cell with In₃Se₄ BSF layer, respectively and it is observed that all PV parameters follow the same trend as like as CdS BSF layer. In Fig. 11c for In₃Se₄ layer it is found that there is no dependency of series resistance on V_{OC} and J_{SC} . The FF and PCE are decreased from 85.11 to 38% to 56.81 and 25.35%, respectively with increasing R_s from 0 to 5 Ω . It is also found in Fig. 11d that V_{OC} and J_{SC} are independent with shunt resistance (R_{sh}). At first FF and PCE are reduced to 83.93 and 37.40%, respectively but with further increasing of R_{sh} they are slightly improved to 85 and 37.89%, respectively up to 10 K Ω .

3.7. The optimized solar cell structure

The optimized PCE of the PEDOT:PSS/n-Si heterojunction solar cell is 22.46%. The efficiency of the solar cell increases to 30.94%

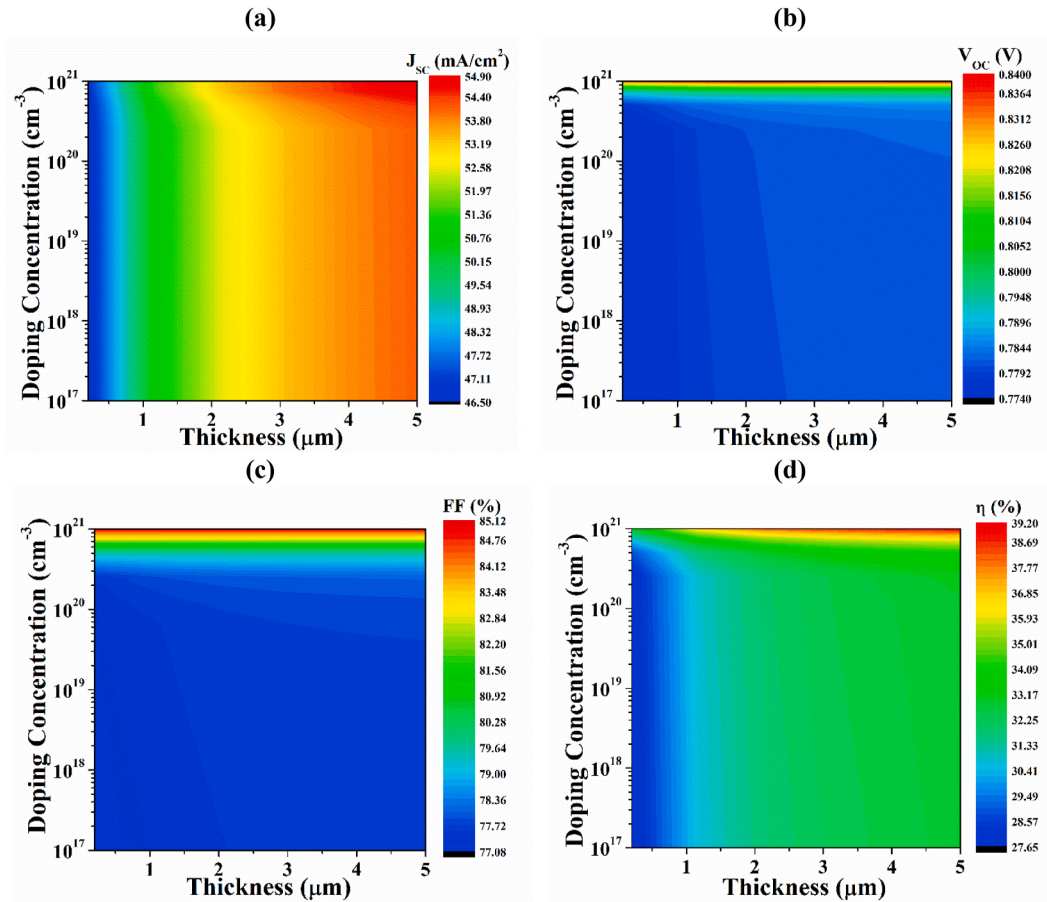


Fig. 8. Variation of PV parameters with respect to thickness and carrier concentration of In_3Se_4 BSF layer: (a) J_{SC} , (b) V_{OC} (c) FF and (d) Efficiency (η).

with the insertion of highly conductive CdS buffer layer. The PCE of the solar cell further increases to 38% with the insertion of In_3Se_4 buffer layer that also acts as bottom absorber layer. The summarized PV parameters of PEDOT:PSS/n-Si heterojunction solar cells with and without CdS and In_3Se_4 BSF layer, respectively are shown in Table 4.

4. Conclusions

We demonstrate the highly efficient PEDOT:PSS/n-Si heterojunction solar cells by SCAPS software using experimental data. The simulations reveals that the incorporation of CdS and In_3Se_4 chalcogenide compounds as back surface field (BSF) layers in the solar cell structure significantly improves the power conversion efficiency (PCE) of the PEDOT:PSS/n-Si heterojunction solar cells. The optimized PCE of the PEDOT:PSS/n-Si solar cell without any BSF layer is about 22.46%. The CdS BSF layer increases the PCE of the solar cell to 30.94% with $V_{\text{OC}} = 0.89$ V, $J_{\text{SC}} = 44.02 \text{ mA}/\text{cm}^2$ and FF = 78.92%, respectively. On the other hand, the insertion of In_3Se_4 BSF layer which also acts as bottom absorber layer enhances PCE of the solar cell to 38% with $V_{\text{OC}} = 0.84$ V, $J_{\text{SC}} = 53.22 \text{ mA}/\text{cm}^2$ and FF = 85.11%, respectively. This study reveals that both CdS and In_3Se_4 compounds as BSF layers have the potential for the enhancement of efficiency of PEDOT:PSS/n-Si heterojunction solar cells in future.

Author statement

The Authors hereby grants the Journal "Superlattices and Microstructures" full and exclusive rights to the manuscript, all revisions, and the full copyright. The Journal "Superlattices and Microstructures" rights include but are not limited to the following: (1) to reproduce, publish, sell, and distribute copies of the manuscript, selections of the manuscript, and translations and other derivative works based upon the manuscript, in print, audio-visual, electronic, or by any and all media now or hereafter known or devised; (2) to license reprints of the manuscript to third persons for educational photocopying; (3) to license others to create abstracts of the manuscript and to index the manuscript; (4) to license secondary publishers to reproduce the manuscript in print, microform, or any computer-readable form, including electronic on-line databases; and (5) to license the manuscript for document delivery. These

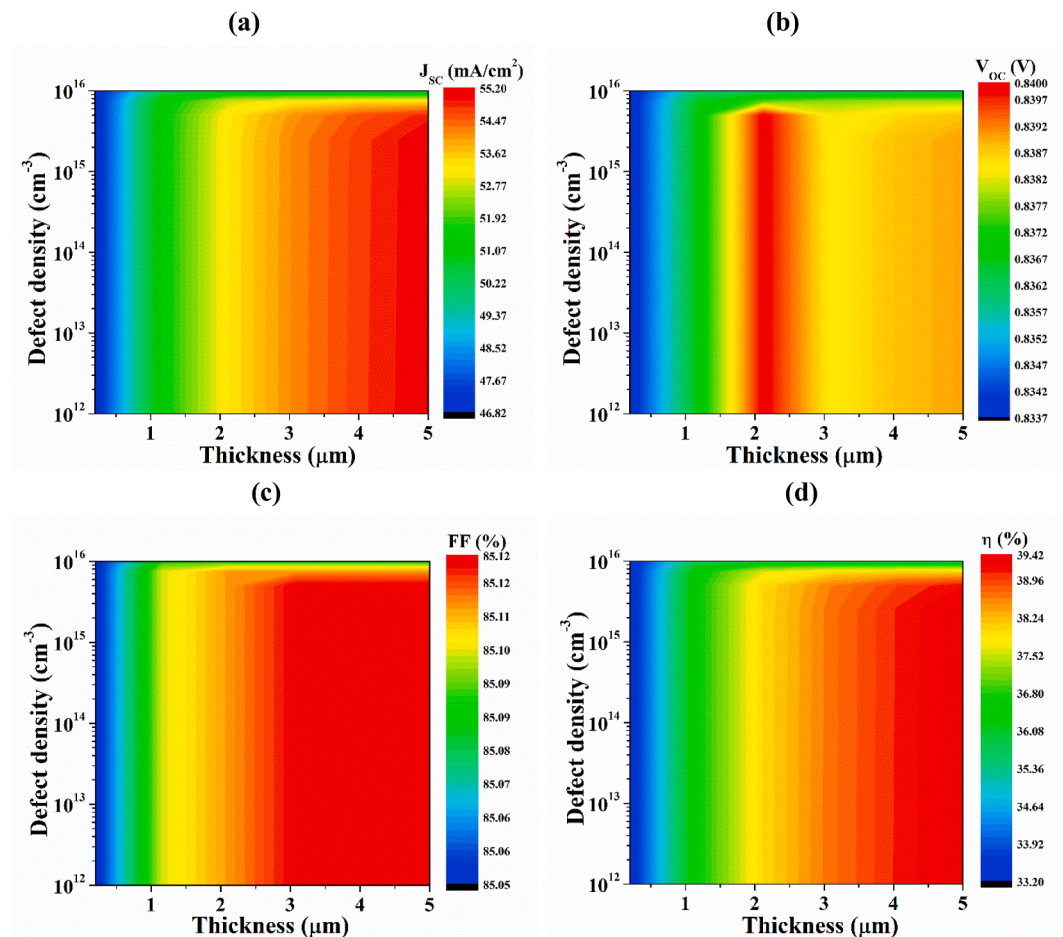


Fig. 9. Variation of PV parameters with respect to thickness and defect density of In_3Se_4 BSF layer: (a) J_{SC} , (b) V_{OC} , (c) FF and (d) Efficiency (η).

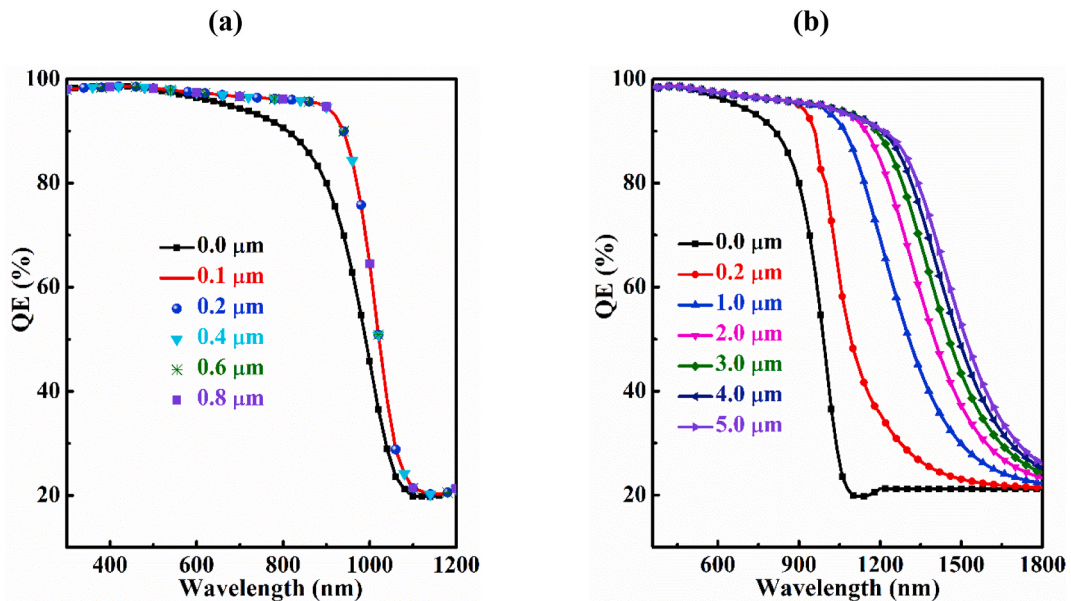


Fig. 10. The effect of (a) CdS and (b) In_3Se_4 BSF layers on quantum efficiency of PEDOT:PSS/n-Si/(CdS or In_3Se_4) solar cell.

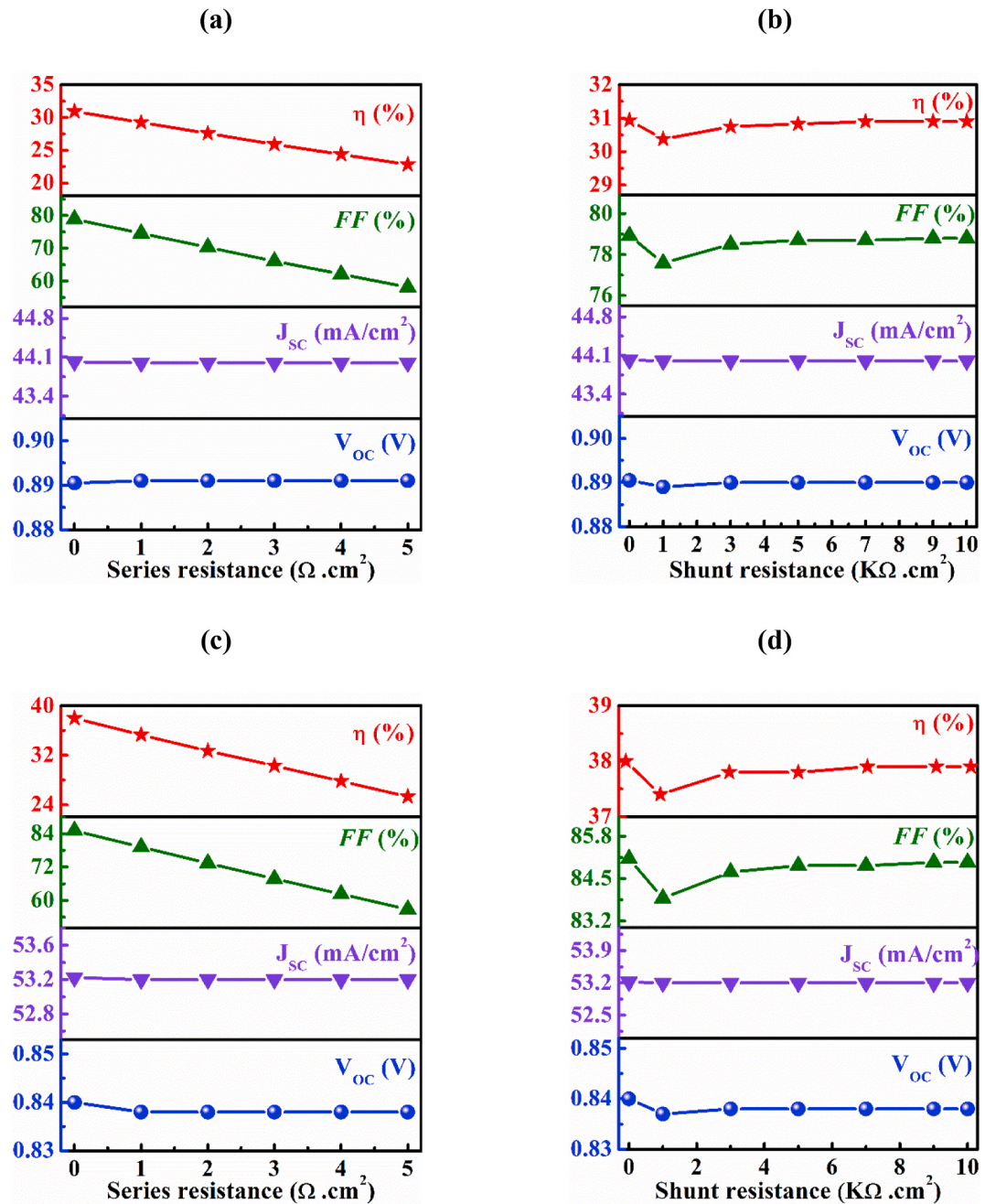


Fig. 11. Effect of series and shunt resistance on PEDOT:PSS/Si solar cell with CdS (a & b) and In_3Se_4 (c & d) BSF layers, respectively.

Table 4

The optimized PV parameters for PEDOT:PSS/n-Si solar cell with and without BSF layer.

Device Structure	J_{sc} (mA/cm^2)	V_{oc} (V)	FF (%)	η (%)
p-PEDOT:PSS/n-Si	41.65	0.65	83.55	22.46
p-PEDOT:PSS/n-Si/ n^+ -Cds	44.02	0.89	78.92	30.94
p-PEDOT/n-Si/ n^+ - In_3Se_4	53.22	0.84	85.11	38.00

exclusive rights run the full term of the copyright, and all renewals and extensions thereof.

I hereby accept the terms of the above Author Statement and I sign on behalf of the authors.

Declaration of competing interest

The authors declare that they have no known competing financial interests or personal relationships that could have appeared to influence the work reported in this paper.

Acknowledgements

This study was partially supported by a grant #A-1495/5/52/UGC/FE/1/2018–2019 of University Grants Commission (UGC), Bangladesh. The authors highly appreciate Dr. Marc Burgelman, University of Gent, Belgium, for providing SCAPS simulation software.

References

- [1] S. Avasthi, S. Lee, Y.-L. Loo, J.C. Sturm, Role of majority and minority carrier barriers silicon/organic hybrid heterojunction solar cells, *Adv. Mater.* 23 (2011) 5762–5766, <https://doi.org/10.1002/adma.201102712>.
- [2] J. Hossain, T. Ohki, K. Ichikawa, K. Fujiyama, K. Ueno, Y. Fujii, T. Hanajiri, H. Shirai, Investigating the chemical mist deposition technique for poly(3,4-ethylenedioxythiophene):poly(styrene sulfonate) on textured crystalline-silicon for organic/crystalline-silicon heterojunction solar cells, *Jpn. J. Appl. Phys.* 55 (2016), 031601, <https://doi.org/10.7567/JJAP.55.031601>.
- [3] Q. Liu, M. Ono, Z. Tang, R. Ishikawa, K. Ueno, H. Shirai, Highly efficient crystalline silicon/zonylfluorosurfactant-treated organic heterojunction solar cell, *Appl. Phys. Lett.* 100 (2012) 183901, <https://doi.org/10.1063/1.4709615>.
- [4] J. Schmidt, V. Titova, D. Zielke, Organic-silicon heterojunction solar cells: open-circuit voltage potential and stability, *Appl. Phys. Lett.* 103 (2013) 183901, <https://doi.org/10.1063/1.4827303>.
- [5] R. Devkota, Q. Liu, T. Ohki, J. Hossain, K. Ueno, H. Shirai, Solution-processed crystalline silicon double-heterojunction solar cells, *APEX* 9 (2016), 022301, <https://doi.org/10.7567/APEX.9.022301>.
- [6] J. Hossain, Q. Liu, T. Miura, K. Kasahara, D. Harada, R. Ishikawa, K. Ueno, H. Shirai, Nafion-modified PEDOT:PSS as a transparent hole-transporting layer for high-performance crystalline-Si/organic heterojunction solar cells with improved light soaking stability, *ACS Appl. Mater. Interfaces* 8 (2016) 31926–31934, <https://doi.org/10.1021/acsmami.6b10272>.
- [7] S. Funda, T. Ohki, Q. Liu, J. Hossain, Y. Ishimaru, K. Ueno, H. Shirai, Correlation between the fine structure of spin-coated PEDOT:PSS and the photovoltaic performance of organic/crystalline-silicon heterojunction solar cells, *J. Appl. Phys.* 120 (2016), 033103, <https://doi.org/10.1063/1.4958845>.
- [8] Q. Liu, R. Ishikawa, S. Funda, T. Ohki, K. Ueno, H. Shirai, Highly efficient solution-processed poly(3,4-ethylenedioxythiophene):poly(styrenesulfonate)/crystalline-silicon heterojunction solar cells with improved light-induced stability, *Adv. Energy Mater.* 5 (2015) 1500744, <https://doi.org/10.1002/aenm.201500744>.
- [9] J. He, P. Gao, Z. Yang, J. Yu, W. Yu, Y. Zhang, J. Sheng, J. Ye, J.C. Amine, Y. Cui, Silicon/organic hybrid solar cells with 16.2% efficiency and improved stability by formation of conformal heterojunction coating and moisture-resistant capping layer, *Adv. Mater.* 29 (2017) 1606321, <https://doi.org/10.1002/adma.201606321>.
- [10] D. Zielke, R. Gogolin, M.-U. Halbich, C. Marquardt, W. Lövenich, R. Sauer, J. Schmidt, P.E.D.O.T. Large-area, PSS/c-Si heterojunction solar cells with screen-printed metal contacts, *Sol. RRL* 2 (2018) 1700191, <https://doi.org/10.1002/solr.201700191>.
- [11] K. Kasahara, J. Hossain, D. Harada, K. Ichikawa, R. Ishikawa, H. Shirai, Crystalline-Si heterojunction with organic thin-layer (HOT) solar cell module using poly(3,4-ethylenedioxythiophene):poly(styrene sulfonate) (PEDOT:PSS), *Sol. Energy Mater. Sol. Cells* 181 (2018) 60–70, <https://doi.org/10.1016/j.solmat.2017.10.016>.
- [12] S. Mukherjee, R. Singh, S. Gopinathan, S. Murugan, S. Gawali, B. Saha, J. Biswas, S. Lodha, A. Kumar, Solution-processed poly(3,4-ethylenedioxythiophene) thin films as transparent conductors: effect of p-toluenesulfonic acid in dimethyl sulfoxide, *ACS Appl. Mater. Interfaces* 6 (2014) 17792–17803, <https://doi.org/10.1021/am504150n>.
- [13] W. Fang, Z. Ni, P. Wang, C. Xiang, T. Sun, J. Zhang, R. Wang, J. Yang, Y. Yang, The ideal doping concentration of silicon wafer for single junction hybrid n-Si/PEDOT: PSS solar cells with 3.2% elevated PCE and V_{OC} of 620 mV, *J. Mater. Sci. Mater. Electron.* 31 (2020) 6398–6405, <https://doi.org/10.1007/s10854-020-03196-y>.
- [14] B. Chen, J. Chen, Y. Shen, K. Ge, J. Guo, F. Li, H. Liu, Y. Xu, Y. Mai, Magnesium thin film as a doping-free back surface field layer for hybrid solar cells, *Appl. Phys. Lett.* 110 (2017) 133504, <https://doi.org/10.1063/1.4979345>.
- [15] H. Tong, Z. Yang, X. Wang, Z. Liu, Z. Chen, X. Ke, M. Sui, J. Tang, T. Yu, Z. Ge, Y. Zeng, P. Gao, J. Ye, Dual functional electron-selective contacts based on silicon oxide/magnesium tailoring heterointerface band structures while maintaining surface passivation, *Adv. Energy Mater.* 8 (2018) 1702921, <https://doi.org/10.1002/aenm.201702921>.
- [16] Y. Zhang, R. Liu, S.-T. Lee, B. Sun, The role of a LiF layer on the performance of poly(3,4-ethylenedioxythiophene):poly(styrenesulfonate)/Si organic-inorganic hybrid solar cells, *Appl. Phys. Lett.* 104 (2014), 083514, <https://doi.org/10.1063/1.4866968>.
- [17] Y. Zhang, W. Cui, Y. Zhu, F. Zu, L. Liao, S.-T. Lee, B. Sun, High efficiency hybrid PEDOT:PSS/nanostructured silicon Schottky junction solar cells by doping-free rear contact, *Energy Environ. Sci.* 8 (2015) 297–302, <https://doi.org/10.1039/C4EE02282C>.
- [18] J. Hossain, K. Kasahara, D. Harada, A.T.M. Saiful Islam, R. Ishikawa, K. Ueno, T. Hanajiri, Y. Nakajima, Y. Fujii, M. Tokuda, H. Shirai, Barium hydroxide hole blocking layer for front-and-back-organic/crystalline Si heterojunction solar cells, *J. Appl. Phys.* 122 (2017) 55101, <https://doi.org/10.1063/1.4985812>.
- [19] Y. Liu, Z.-G. Zhang, Z. Xia, J. Zhang, Y. Liu, F. Liang, Y. Li, T. Song, X. Yu, S.-T. Lee, B. Sun, High performance nanostructured silicon–organic quasi p–n junction solar cells via low-temperature deposited hole and electron selective layer, *ACS Nano* 10 (2016) 704–712, <https://doi.org/10.1021/acsnano.5b05732>.
- [20] Y. Liu, J. Zhang, H. Wu, W. Cui, R. Wang, K. Ding, S.-T. Lee, B. Sun, Low-temperature synthesis TiO_x passivation layer for organic-silicon heterojunction solar cell with a high open-circuit voltage, *Nanomater. Energy* 34 (2017) 257–263, <https://doi.org/10.1016/j.nanoen.2017.02.024>.
- [21] Y. Zhang, F. Zu, S.-T. Lee, L. Liao, N. Zhao, B. Sun, Heterojunction with organic thin layers on silicon for record efficiency hybrid solar cells, *Adv. Energy Mater.* 4 (2014) 1300923, <https://doi.org/10.1002/aenm.201300923>.
- [22] Y. Han, Y. Liu, J. Yuan, H. Dong, Y. Li, W. Ma, S.-T. Lee, B. Sun, Naphthalene diimide-based n-type polymers: efficient rear interlayers for high performance silicon-organic heterojunction solar cells, *ACS Nano* 11 (2017) 7215–7222, <https://doi.org/10.1021/acsnano.7b03090>.
- [23] C. Reichel, U. Würfel, K. Winkler, H.-F. Schleiermacher, M. Kohlstädter, M. Unmüssig, C.A. Messmer, M. Hermle, S.W. Glunz, Electron-selective contacts via ultra-thin organic interface dipoles for silicon organic heterojunction solar cells, *J. Appl. Phys.* 123 (2018), 024505, <https://doi.org/10.1063/1.5010937>.
- [24] T. Ohki, K. Ichikawa, J. Hossain, Y. Fujii, T. Hanajiri, R. Ishikawa, K. Ueno, H. Shirai, Effect of substrate bias on mist deposition of conjugated polymer on textured crystalline-Si for efficient c-Si/organic heterojunction solar cells, *Phys. Status Solidi A* 213 (2016) 1922–1925, <https://doi.org/10.1002/pssa.201532951>.
- [25] L. Yang, Y. Liu, W. Chen, Y. Wang, H. Liang, Z. Mei, A. Kuznetsov, X. Du, Interface engineering of high efficiency organic-silicon heterojunction solar cells, *ACS Appl. Mater. Interfaces* 8 (2016) 26–30, <https://doi.org/10.1021/acsami.5b10959>.

- [26] K. Yoshikawa, H. Kawasaki, W. Yoshida, T. Irie, K. Konishi, K. Nakano, T. Uto, D. Adachi, M. Kanematsu, H. Uzu, K. Yamamoto, Silicon heterojunction solar cell with interdigitated back contacts for a photoconversion efficiency over 26%, *Nat. Energy* 2 (2017) 17032, <https://doi.org/10.1038/nenergy.2017.32>.
- [27] A.D. Vos, Detailed balance limit of the efficiency of tandem solar cells, *J. Phys. D Appl. Phys.* 13 (1980) 839–846, <https://doi.org/10.1088/0022-3727/13/5/018>.
- [28] A.S. Brown, M.A. Green, Detailed balance limit for the series constrained two terminal tandem solar cell, *Physica E* 14 (2002) 96–100.
- [29] A. Luque, A. Martí, Increasing the efficiency of ideal solar cells by photon induced transitions at intermediate levels, *Phys. Rev. Lett.* 78 (1997) 5014–5017, <https://doi.org/10.1103/PhysRevLett.78.5014>.
- [30] A.S. Brown, M.A. Green, Impurity photovoltaic effect: fundamental energy conversion efficiency limits, *J. Appl. Phys.* 92 (2002) 1329–1336, <https://doi.org/10.1063/1.1492016>.
- [31] M. Schmeits, A.A. Mani, Impurity photovoltaic effect in c-Si solar cells. A numerical study, *J. Appl. Phys.* 85 (1999) 2207–2212, <https://doi.org/10.1063/1.369528>.
- [32] M.F. Rahman, J. Hossain, A. Kuddus, S. Tabassum, M.H.K. Rubel, H. Shirai, A.B.M. Ismail, A novel synthesis and characterization of transparent CdS thin films for CdTe/CdS solar cells, *Appl. Phys. A* 126 (2020) 145, <https://doi.org/10.1007/s10853-020-04578-7>.
- [33] L. Cai, W. Wang, L. Jin, Z. Yao, W. Lin, L. Meng, B. Ai, Z. Liang, Y. Huang, F. Zhang, P.P. Altermatt, H. Shen, 12.29% Low temperature-processed dopant-free CdS/n-Si heterojunction solar cells, *Adv. Mater. Interfaces* 6 (2019) 1900367, <https://doi.org/10.1002/admi.201900367>.
- [34] G. Han, Z.-G. Chen, L. Yang, L. Cheng, K. Jack, J. Drennan, J. Zou, Thermal stability and oxidation of layer-structured rhombohedral In₃Se₄ nanostructures, *Appl. Phys. Lett.* 103 (2013) 263105, <https://doi.org/10.1063/1.4857655>.
- [35] G. Han, Z.-G. Chen, C. Sun, L. Yang, L. Cheng, Z. Li, W. Lu, Z.M. Gibbs, G.J. Snyder, K. Jack, J. Drennan, J. Zou, A new crystal: layer-structured rhombohedral In₃Se₄, *CrystEngComm* 16 (2014) 393, <https://doi.org/10.1039/C3CE41815D>.
- [36] J. Hossain, M. Julkarnain, B.K. Mondal, M.A. Newaz, K.A. Khan, Unveiling the electrical and thermoelectric properties of highly degenerate indium selenide thin films: indication of In₃Se₄ phase, *Mater. Res. Express* 6 (2019) 126421, <https://doi.org/10.1088/2053-1591/ab5ac1>.
- [37] B.K. Mondal, M.A. Newaz, M.A. Rashid, K.M. Hossain, S.K. Mostaque, M.F. Rahman, M.H.K. Rubel, J. Hossain, Electronic structure of In_{3-x}Se₄ electron transport layer for chalcogenide/p-Si heterojunction solar cells, *ACS Omega* 4 (2019) 17762, <https://doi.org/10.1021/acsomega.9b02210>.
- [38] G. Han, Q. Gu, L. Yang, Z.-G. Chen, J. Zou, A new indium selenide phase: controllable synthesis, phase transformation and photoluminescence properties, *J. Mater. Chem. C* 7 (2019) 13573–13584, <https://doi.org/10.1039/C9TC04635F>.
- [39] Z. Lin, Q. He, A. Yin, Y. Xu, C. Wang, M. Ding, H.-C. Cheng, B. Papandrea, Y. Huang, X. Duan, Cosolvent approach for solution processable electronic thin films, *ACS Nano* 9 (4) (2015) 4398–4405, <https://doi.org/10.1021/acsnano.5b00886>.
- [40] M. Burgelman, J. Verschraegen, S. Degraeve, P. Nollet, Modeling thin-film PV devices, *Prog. Photovoltaics Res. Appl.* 12 (2004) 143–153, <https://doi.org/10.1002/pip.524>.
- [41] O.K. Simya, A. Mahabobbatcha, K.A. Balachander, A comparative study on the performance of kesterite based thin film solar cells using SCAPS simulation program, *Superlattice. Microst.* 82 (2015) 248–261, <https://doi.org/10.1016/j.spmi.2015.02.020>.
- [42] H. Movla, Optimization of the CIGS based thin film solar cells: numerical simulation and analysis, *Optik* 125 (2014) 67–70, <https://doi.org/10.1016/j.jleo.2013.06.034>.
- [43] A. Kuddus, M.F. Rahman, S. Ahmed, J. Hossain, A.B.M. Ismail, Role of facile synthesized V₂O₅ as hole transport layer for CdS/CdTe heterojunction solar cell: validation of simulation using experimental data, *Superlattice. Microst.* 132 (2019) 106168, <https://doi.org/10.1016/j.spmi.2019.106168>.
- [44] A.B. Prakoso, Rusli, Z. Li, C. Lu, C. Jiang, Design guideline for Si/organic hybrid solar cell with interdigitated back contact structure, *Semicond. Sci. Technol.* 33 (2018), 035016, <https://doi.org/10.1088/1361-6641/aaa917>.
- [45] C.-H. Ho, Y.-J. Chu, Bending photoluminescence and surface photovoltaic effect on multilayer InSe 2D microplate crystals, *Adv. Optical Mater.* 3 (2015) 1750–1758, <https://doi.org/10.1002/adom.201500390>.
- [46] J. Hossain, M. M. A. Moon, B. K. Mondal, M. A. Halim, Design Guidelines for a Novel High-Purity Germanium (HPGe) Based High Efficiency Npp⁺ Heterojunction Solar Cells, arXiv:2009.13948 [physics.app-ph].
- [47] M.A. Green, Intrinsic concentration, effective densities of states, and effective mass in silicon, *J. Appl. Phys.* 67 (1990) 2944, <https://doi.org/10.1063/1.345414>.
- [48] M.M.A. Moon, M.H. Ali, M.F. Rahman, A. Kuddus, J. Hossain, A.B.M. Ismail, Investigation of thin-film p-BaSi₂/n-CdS heterostructure towards semiconducting silicide based high efficiency solar cell, *Phys. Scripta* 95 (2020), 035506, <https://doi.org/10.1088/1402-4896/ab49e8>.
- [49] M.M.A. Moon, M.H. Ali, M.F. Rahman, J. Hossain, A.B.M. Ismail, Design and simulation of FeSi₂ based novel heterojunction solar cells for harnessing visible and near-infrared light, *Phys. Status Solidi A* 217 (2020) 1900921, <https://doi.org/10.1002/pssa.201900921>.
- [50] T. Watahiki, Y. Kobayashi, T. Morioka, S. Nishimura, D. Niinobe, K. Nishimura, H. Tokioka, M. Yamamuka, Analysis of short circuit current loss in rear emitter crystalline Si solar cell, *J. Appl. Phys.* 119 (2016) 204501, <https://doi.org/10.1063/1.4951003>.
- [51] M. Lu, S. Bowden, U. Das, R. Birkemire, Interdigitated back contact silicon heterojunction solar cell and the effect of front surface passivation, *Appl. Phys. Lett.* 91 (2007), 063507, <https://doi.org/10.1063/1.2768635>.
- [52] J. Hossain, B.K. Mondal, S.K. Mostaque, S.R.A. Ahmed, H. Shirai, Optimization of multilayer anti-reflection coatings for efficient light management of PEDOT: PSS/C-Si heterojunction solar cells, *Mater. Res. Express* 7 (2020), 015502, <https://doi.org/10.1088/2053-1591/ab5ac7>.
- [53] K.R. McIntosh, L.P. Johnson, Recombination at textured silicon surfaces passivated with silicon dioxide, *J. Appl. Phys.* 105 (2009) 124520, <https://doi.org/10.1063/1.3153979>.
- [54] N. Bensedik, B. Belkacemi, F. Boukabrine, K. Ameur, H. Mazari, A. Boumesjed, N. Benyahya, Z. Benamara, Numerical study of AgInTe₂ solar cells using SCAPS, *Advances in Materials and Processing Technologies*, 2020, <https://doi.org/10.1080/2374068X.2020.1833401>.
- [55] S. K. Mostaque, B. K. Mondal, J. Hossain, Simulation approach to reach the SQ limit in CIGS-based dual-heterojunction solar cell, (submitted to Progress in photovoltaics).
- [56] S. Ahmed, A. Aktar, J. Hossain, A.B.M. Ismail, Enhancing the open circuit voltage of the SnS based heterojunction solar cell using NiO HTL, *Sol. Energy* 207 (2020) 693–702, <https://doi.org/10.1016/j.solener.2020.07.003>.
- [57] S. Asahi, H. Teranishi, K. Kusaki, T. Kaiju, T. Kita, Two-step photon up-conversion solar cells, *Nat. Commun.* 8 (2017) 1–9, <https://doi.org/10.1038/ncomms14962>.